Physical Modeling of Transient Enhanced Diffusion and Dopant Deactivation via Extended Defect Evolution

Alp H. Gencer, Srinivasan Chakravarthi and Scott T. Dunham
Dept. of Electrical and Computer Eng., Boston University, Boston MA 02215

Abstract— Simulation of ion implant annealing requires adequate models for a range of processes, including deactivation of dopants and transient enhanced diffusion. It is now well understood that extended defects ({311} defects, dislocation loops, BICs, arsenic precipitates, etc.) play a central role in all these processes. We have developed a fundamental model which can account for the behavior of a broad range of extended defects, as well as their interactions with each other. We have successfully applied and parameterized our model to a range of systems and conditions, some of which are presented in this paper. We also present how these processes couple with each other, as well as standard coupled dopant diffusion, by terms of a simple MOSFET structure.

I. Introduction

As VLSI processing continues to push towards smaller junction depths and higher dopant concentrations, transient enhanced diffusion (TED) and dopant deactivation kinetics become increasingly important. However, these processes involve formation and evolution of extended defects, which are not well-modeled using conventional continuity equation approaches. The reason is that the behavior of extended defects depends on their size distribution at any given time and are thus hard to integrate into a process simulator.

Numerous types of extended defect form during annealing of ion implantation. In silicon self-implanted and annealed samples interstitial-type extended defects are observed. These defects are primarily {311} defects for low-dose, sub-amorphizing implants and dislocation loops for high dose implants. These extended defects act to store excess interstitials generated by implantation, reducing the initial supersaturation, but greatly prolonging the time period over which TED lasts. In addition, it has been observed that even well below solubility the peaks of implanted boron profiles remain immobile under TED conditions, a behavior which has been attributed to the formation of boron-interstitial clusters (BICs). Above

solubility, arsenic also becomes immobile and inactive via clustering/precipitation, incorporating vacancies (or injecting interstitials) during the process. These extended defects not only form individually, but they also interact with each other through changes in point defect and solute concentrations. It has become clear from these and other related observations that extended defects play a primary role in TED and that therefore predictive modeling of TED requires the use of well-founded physical models for these aggregation processes.

We have developed a general framework in which all of these effects can be modeled in a consistent and fundamental way, and have applied our model successfully to a range of conditions. We use a moment-based approach to modeling of the size distribution of extended defects (Reduced Kinetic Precipitation Model) to consider the evolution of each extended defect distribution ({311} defects, dislocation loops, BICs, arsenic precipitates, etc.) and how they vary with spatial location, as well as their interactions with standard coupled dopant/defect diffusion and each other.

II. Model for Extended Defects and Dopant Deactivation

A. Energetics of the model

We model the evolution of an extended defect population or dopant clusters by explicitly considering precipitates of different sizes as independent species (f_n) and account for their kinetics by considering the attachment and emission of solute atoms.[1]

The driving force for precipitation is the minimization of the free energy of the system, where the free energy of a size n extended defect is given by:

$$\Delta G_n = -nkT \ln \frac{C_A}{C_{ss}} + \Delta G_n^{exc} \qquad (1)$$

Here, C_{ss} is the solid solubility of the solute (interstitials or dopant atoms). ΔG_n^{exc} is the combined excess surface and strain energy of a size n precipitate. We assume ΔG_n^{exc} to have a polynomial form:

$$\Delta G_n^{exc} = a_0 n^{\beta_0} + a_1 n^{\beta_1} + a_2 n^{\beta_2}, \qquad (2)$$

It can be argued that $\beta_0 = 0.5$ for dislocation loops since these are disc-like defects and the excess surface energy will essentially be proportional to the perimeter of

the disc as the defect size increases. By the same argument, $\beta_0 = 2/3$ for dopant precipitates, which are assumed to be spherical in shape.

The energetics of the system changes if the precipitates consist of more than one species, such as a boron precipitate incorporating interstitials ($B_n I_m$). It is clear that a dopant with atomic volume smaller than silicon will tend to incorporate interstitials to minimize their free energy, and the converse is true for dopants with an atomic volume larger than silicon. In this case, the free energy is given by:[2]

$$\Delta G_{n,m} = \Delta G_n^{\text{exc}} + \Delta G_{n,m}^{\text{stress}} - nkT \log(C_A/C_{\text{ss}}) \\ -mkT \log(C_I/C_I^*), \tag{3}$$

where n is the number of dopant atoms, m is the net number of incorporated interstitials (negative in case of incorporation of vacancies or injection of interstitials). The stress energy can be found from the elasticity theory by assuming a parabolic behavior around an equilibrium point:

$$\Delta G_{n,m}^{\text{stress}} = H_n + \frac{\alpha}{n}(m - \gamma n)^2. \tag{4}$$

If there was no point defect supersaturation, the optimum number of incorporated interstitials would be $m^* = \gamma n$. However, when we have an supersaturation, the optimum number of point defects incorporated can be found from minimizing the free energy to be:

$$m^* = n\left(\gamma + \frac{kT}{2\alpha} \log(C_I/C_I^*)\right), \tag{5}$$

which leads to an effective solid solubility of:

$$C_{\text{ss}}^{\text{eff}} = C_{\text{ss}}\left(\frac{C_I}{C_I^*}\right)^{-\gamma} \exp\left[-\frac{kT}{4\alpha}\left(\log(C_I/C_I^*)\right)^2.\right] \tag{6}$$

B. Kinetics of the model

The main reaction in the system is the attachment and emission of solute atoms to and from extended defects. I_n, the net growth rate from size n to $n+1$, may be written as:

$$I_n = D\lambda_n \left(C_A f_n - C_n^* f_{n+1}\right). \tag{7}$$

The kinetic growth factor, λ_n, incorporates effects of both diffusion to the precipitate/silicon interface and the reaction at the interface. λ_n is calculated based on solving the steady-state diffusion equation in the neighborhood of the defect, taking the defect shape into account. C_n^* represents the interstitial concentration in equilibrium with a size n defect:

$$C_n^* = C_{\text{ss}}^{\text{eff}} \exp\left(\frac{\Delta G_{n+1}^{\text{exc}} - \Delta G_n^{\text{exc}}}{kT}\right) \tag{8}$$

To integrate the our model into a diffusion equation solver, we follow the moment-based approach[3] and keep track of only the lowest three *moments* of the distribution

($m_i = \sum_{n=2}^{\infty} n^i f_n$, where $i = 0, 1, 2$) with an appropriate closure assumption. In particular, the closure assumption used is that the distribution is the one that minimizes the free energy, given the moments. The resulting system has the following set of continuity equations:

$$\begin{aligned} \frac{\partial m_0}{\partial t} &= I_1 \\ \frac{\partial m_1}{\partial t} &= 2I_1 + \sum_{n=2}^{\infty} I_n \\ \frac{\partial m_2}{\partial t} &= 4I_1 + \sum_{n=2}^{\infty} I_n(2n+1) \\ \frac{\partial C_A}{\partial t} &= -2I_1 - \sum_{n=2}^{\infty} I_n + \text{diffusion terms} \end{aligned} \tag{9}$$

Note that with the closure assumption, the sums over the I_n can be calculated from the three moments,[3] but require the solution of a non-linear equation system at every time step and each grid point. To make the simulation computationally efficient, the sums are pre-tabulated for a range of m_i values and interpolation from these values is used during the simulation.[4]

III. MODELING OF {311} DEFECTS AND DISLOCATION LOOPS

The formation and evolution of {311} defects can be modeled successfully using the Kinetic Precipitation Model[1]. Modeling of dislocation loops, however, requires more care, since it has been observed that {311} defects transform into dislocation loops under certain conditions. We believe that this transformation is the primary mechanism for formation of dislocation loops.

We extended our model for {311} defects to dislocation loops by assuming that there are two population of extended defects, which can interact with each other. We assumed that for smaller sizes it was energetically more favorable to stay as a {311} defect, but above a certain size it was more favorable to transform into a dislocation loop. Our simulations gave a cross-over around $n = 2200$. The transfer rate from {311} defects into dislocation loops can be expressed as:

$$\frac{D_I}{b^2}\left[f_n^{\{311\}} - f_n^{\text{loop}} \exp\left(-\frac{\Delta G_n^{\{311\}} - \Delta G_n^{\text{loop}}}{kT}\right)\right] \tag{10}$$

where b is a "capture distance." We found a value of $20\,\mu$m for b. Thus the transfer from {311} defects into dislocation loops is a rather slow process.

Pan $et\ al.$[5] implanted 1×10^{16} cm^{-2} Si into silicon at 50 keV and annealed the samples at 850°C and 1000°C. They measured the resulting dislocation loop distributions using TEM. The parameters for {311} defects were from previous work.[1] It can be argued that C_{ss} for loops should be just C_I^*, since an infinite size perfect loop is nothing but an extra plane in silicon. For partial loops
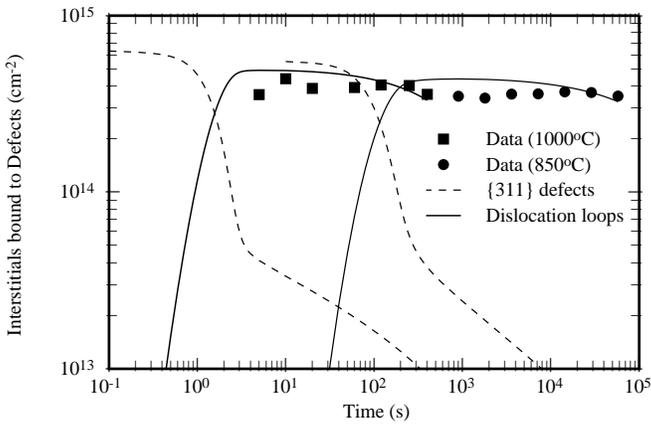
Fig. 1. Evolution of density of interstitials in extended defects (m_1) and comparison to model. Data from Pan et al.[5] for 1×10^{16} cm^{-2} Si implant at 50 keV with anneals at 1000°C and 850°C.
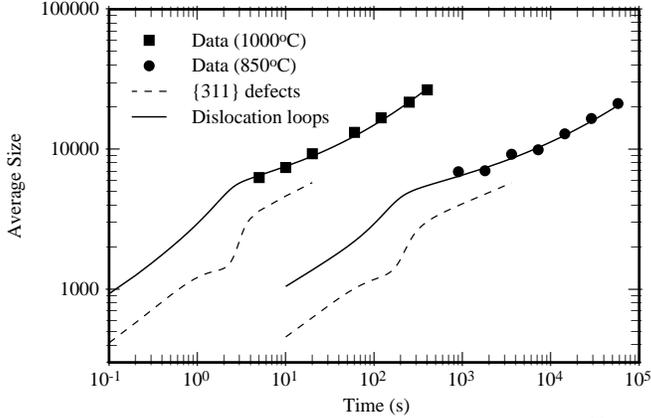

Fig. 2. Evolution of average defect size (m_1/m_0) for 1×10^{16} cm^{-2} Si implants at 50 keV and comparison to data from Pan et al.[5]

Fig. 3. Boron TED and formation of BICs. 2×10^{14} cm^{-2} Si implants at 40 keV and comparison to data from Intel.

Fig. 4. Loop formation due to interstitials injected from deactivation of a high dose, laser annealed As implant. Data from Dokumaci et al.[7] and comparison to model prediction.

C_{ss} should be slightly higher, but small changes in C_{ss} had no significant effect in our simulation results.

Our results show that we were able to correctly model the evolution of the system and transformation of {311} defects into dislocation loops (Fig. 1), as well as the correct Ostwald ripening behavior (Fig. 2). We were also able to get similar matches for data by Lui et al.,[6] which included longer anneals and thus led to substantial loop dissolution.

The relatively slow dissolution rate of dislocation loops stems from the facts that they can grow very large and C_{ss} for loops is equal to C_I^*. This results in C_n^* for loops being close to C_I^*, so that they sustain only a small super-saturation of interstitials. Since these loops are deep in the substrate and sustain only a minimal super-saturation, the flux to the surface is small and thus dissolve they slowly.

IV. Modeling of Dopant Deactivation and TED

Using the same modeling approach, we were also able to get a good match to TED data from Intel. Looking at the evolution of 40 keV 2×10^{14} cm^{-2} B implants, we were able to match the solid solubility decrease due to the interstitial supersaturation, as well as the amount of TED
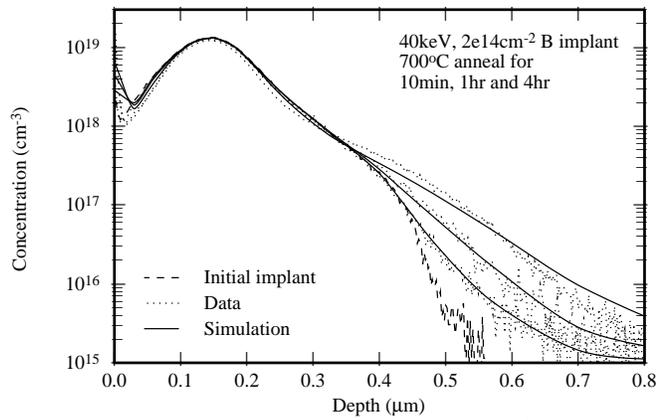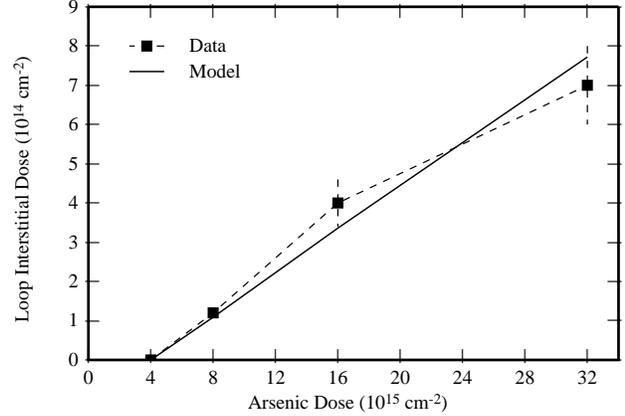
observed (Fig. 3). The formation of boron-interstitial complexes is the driving force for this behavior and the ripening of {311} defects controls the interstitial super-saturation.

We also applied our model to arsenic deactivation with loop formation. Dokumaci et al.[7] implanted As at doses in the range 4×10^{15}–3.2×10^{16} cm^{-2} and laser annealed the surface to get a box-shaped profile. They then annealed the samples at 750°C for 2 hr and measured the loop density by TEM, which formed because As injected interstitials during precipitation. Our simulations show a good fit to their data on the number of interstitials bound to loops (Fig. 4). The simulations also predicted that there would be no observable loops for the smallest dose, as suggested by the data.

V. Simulation of an MOSFET

To demonstrate the interactions between all types of extended defects mentioned ({311} defects, dislocation loops, BICs and arsenic precipitates), we have simulated a typical MOSFET structure. Figures 5 and 6 show simulation results for a vertical cross-section through the S/D extension region of an LDD-MOSFET. The channel doping was formed with a 30 keV, 3×10^{13} cm^{-2} B implant
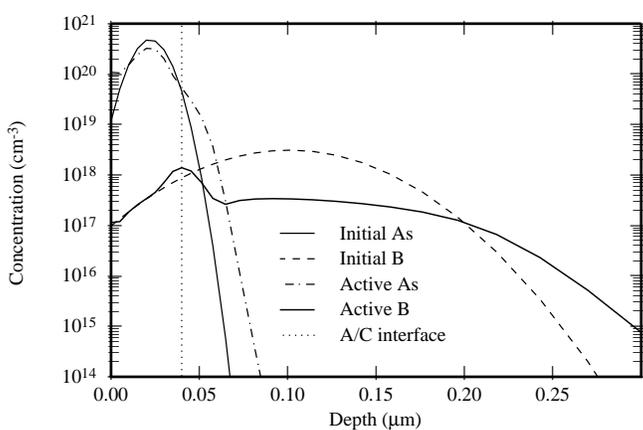
Fig. 5. Simulation of a vertical cross-section through an MOSFET. The initial profiles were obtained using 30 keV 3×10^{13} cm^{-2} boron followed by 25 keV 1×10^{15} cm^{-2} arsenic implantation. Even after a 1 s anneal at 800°C the junction depth moves to $0.07\,\mu$m from $0.05\,\mu$m.
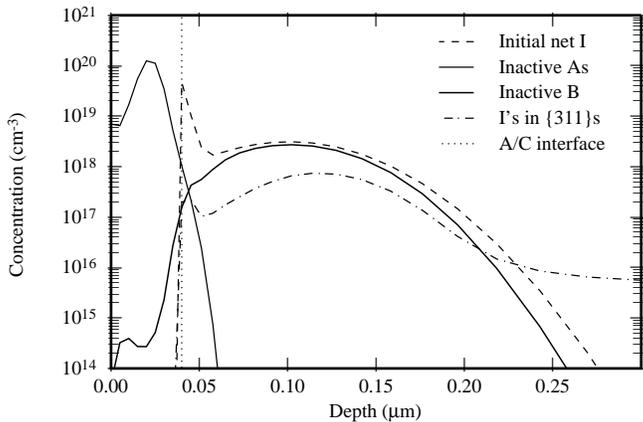

Fig. 6. Inactive dopant concentrations and number of interstitials bound to extended defects under the same conditions as above. The extended defects are primarily {311} defects in the size range 4-5nm.

and the source extension region was formed with a 25 keV, 1×10^{15} cm^{-2} As implant, which gives a projected junction depth of $0.05\,\mu$m.

It is evident that even after only a 1 s anneal at 800°C, substantial profile movement of the As implant has occurred. {311} defects form in the EOR region, but never get the chance to grow to dislocation loops as the implant is very close to the surface. Arsenic-vacancy clusters also form and sustain an interstitial super-saturation in the region close to the surface. Boron-interstitial clusters, which also form during the process, make a portion of the boron peak immobile.

VI. Summary

In summary, we were able to model the formation and evolution of dislocation loops by extending our model for {311} defects to a system with two distributions and accounting for the transfer between {311} defects and dislocation loops. We also extended out model to formation of dopant precipitates with incorporation of point defects. Not only were we able to model individual systems, but

also accounted for cases where a combination of the processes were occurring, such as boron interstitial cluster kinetics with {311} defect formation, arsenic deactivation with dislocation loop formation, or all of them. We believe that our model provides a unified and fundamental approach to all aspects of extended defect formation and evolution.

References

[1] A.H. Gencer and S.T. Dunham, *J. Appl. Phys.* **81**, 631 (1997).
[2] I. Clejan and S.T. Dunham, in **Process Physics and Modeling in Semiconductor Technology**, 398 (1996).
[3] I. Clejan and S.T. Dunham, *J. Appl. Phys.* **78**, 7327 (1995).
[4] A.H. Gencer. *DOPDEES User's Manual* (1996).
[5] G.Z. Pan, K.N. Tu, and S. Prussin, *Appl. Phys. Lett.* **68**, 1654 (1996).
[6] J. Lui, M.E. Law, and K.S. Jones, *Solid State Electronics* **38**, 1305 (1995).
[7] Ö. Dokumacı, P. Rousseau, S. Luninng, V. Krishnamoorthy, K.S. Jones, and M.E. Law, *J. Appl. Phys.* **78**, 828 (1995).